CHINESE OPTICS LETTERS

Vol. 23, No. 1 | January 2025

Temperature sensing based on Lorentz resonance and Fano resonance excited in a thin-walled SiO_2 hollow microrod resonator

Binbin Yang (杨彬彬)[1], Zhaofeng Kang (康朝烽)[1], Tianci Chen (陈天赐)[1], Jun Zhang (张 军)[1], Di Tang (唐 荻)[1], Lei Zhang (张 磊)[1], Keyi Wang (王克逸)[1*], and Yu Yang (杨 煜)[2**]

[1] Department of Precision Machinery and Precision Instrumentation, University of Science and Technology of China, Hefei 230026, China

[2] School of Electrical Engineering and Automation, Hefei University of Technology, Hefei 230009, China

*Corresponding author: kywang@ustc.edu.cn

**Corresponding author: yangyu_hfut@hfut.edu.cn

Received March 27, 2024 | Accepted July 15, 2024 | Posted Online February 4, 2025

A highly sensitive temperature sensor was developed using a thin-walled SiO_2 hollow microrod resonator (SHMR) to excite Lorentz resonance and Fano resonance. The SHMR has a high Q factor (3.16×10^7) and concise resonance modes. Moreover, the SHMR has a small wall thickness, which can effectively improve the sensitivity of the temperature sensor. The experimental results show that the sensitivity reaches 24.78 pm/°C under Lorentz resonance and further improves to 31.28 pm/°C under Fano resonance. By further reducing the wall thickness of the SHMR, the sensitivity under Lorentz resonance is increased to 34.34 pm/°C. The sensor in this study has the advantages of low cost, simple structure, high sensitivity, and satisfactory repeatability.

Keywords: whispering-gallery-mode microresonator; whispering-gallery-mode spectral simplification; Lorentz resonance; Fano resonance; temperature sensing; high sensitivity sensing.

DOI: 10.3788/COL202523.011201

1. Introduction

In recent years, whispering-gallery-mode (WGM) optical microresonators with a high Q factor and small volume modes have received considerable attention from researchers[1], in which typical resonances excited generally have a Lorentz line shape. WGM optical microresonators demonstrate excellent performance in a variety of basic research and practical applications such as nonlinear optics[2], optical communication and precision measurements[3], and various sensors[4–10]. Common WGM microresonators, such as microspheres, microbottles, and microbubbles, have an extremely rich and dense mode spectrum[11–14], which is a disadvantage for various microresonator sensing applications based on mode tracking and recognition. Therefore, researchers have explored various methods to suppress excessive resonance modes to simplify the WGM spectrum, including changing the diameter of the coupling tapered fiber[15], adjusting the coupling position between the tapered fiber and the microresonator[12], and introducing defects on the surface of the microresonator[16,17]. However, such methods are either difficult to repeat or expensive to implement and may sacrifice the quality factor of the microresonator. Starting from the fabrication process, we obtain WGM microresonators with a concise resonant spectrum (few resonant modes) by reducing the axial width and increasing the surface curvature of the microresonator. This method is simple and effective, and most importantly, it does not sacrifice the optical performance of the microresonator.

The SiO_2 hollow microrod resonator (SHMR) in this study has considerable advantages for sensing applications. The SHMR not only facilitates mode tracking and recognition but also effectively improves measurement sensitivity because our preparation process makes it more sensitive to temperature changes, whereas the sensitivity of temperature sensors based on ordinary SiO_2 is generally low[18–22]. Most researchers who are devoted to improving the temperature-sensing sensitivity of SiO_2 microresonators are willing to change the thermo-optic coefficient of the microresonator by combining it with thermal-sensitive materials (polydimethylsiloxane[23,24] and polymethyl methacrylate[25]). Although such methods can improve sensitivity, they have high manufacturing costs and complex processes, and can increase transmission loss and reduce the Q factor of the microresonators.

In addition, more and more researchers have utilized the Fano effect generated by the destructive interference between the discrete modes in the microresonator and the continuous modes of the background light[26] to excite the ideal Fano resonance in the WGM microresonator, which has been widely applied to refractive index sensing[27,28]. The Fano resonance spectrum has sharp resonance peaks[29], which can effectively improve the measurement sensitivity of the refractive index sensing system. Without using any other auxiliary components, we excited a stable asymmetric Fano line shape by adjusting the coupling position between the tapered optical fiber and the SHMR, which is applied to temperature sensing, effectively improving the sensitivity of the sensor.

In this study, we fabricated a high-Q-factor (3.16×10^7) millimeter-scale thin-walled SHMR with a concise resonant spectrum, which facilitates mode tracking and recognition. Moreover, the SHMR has a small wall thickness, which can significantly improve the sensitivity of ordinary SiO_2 microresonator sensors, so that the sensitivity under Lorentz resonance reaches 24.78 pm/°C. Using the Fano resonance excited in the SHMR for temperature sensing, the sensitivity is improved to 31.28 pm/°C. Further reducing the wall thickness of the SHMR, we increased the sensitivity under Lorentz resonance to 34.34 pm/°C.

2. Principle

Changes in ambient temperature can cause changes in the size and refractive index of the microresonator, which will change the optical path of the microresonator and cause a shift in the resonant spectrum. The relationship between the resonant wavelength λ and the temperature variation ΔT is as follows[30]:

$$\lambda(\Delta T) \cong \lambda_0 \left[1 + \left(\frac{\mathrm{d}R}{\mathrm{d}T}/R + \frac{\mathrm{d}n}{\mathrm{d}T}/n_0\right)\Delta T\right], \tag{1}$$

where λ_0 is the resonant wavelength of the microresonator at the initial temperature, $(\mathrm{d}R/\mathrm{d}T)/R$ is the thermal expansion coefficient of the microresonator, R is the radius of the microresonator, $(\mathrm{d}n/\mathrm{d}T)/n_0$ is the thermo-optic coefficient of the microresonator, and n_0 is the refractive index of the microresonator. From Eq. (1), it can be concluded that the variation in the resonant wavelength of the microresonator caused by temperature changes is as follows[31]:

$$\Delta\lambda = \lambda_0 \left(\frac{\mathrm{d}R}{\mathrm{d}T}/R + \frac{\mathrm{d}n}{\mathrm{d}T}/n_0\right)\Delta T. \tag{2}$$

SiO_2 has a positive thermal expansion coefficient ($1.19 \times 10^{-5}\ \mathrm{K}^{-1}$) and thermo-optic coefficient ($5.5 \times 10^{-7}\ \mathrm{K}^{-1}$)[25], so the resonance spectral lines are redshifted (shifted toward longer wavelengths) as the temperature increases. The thermal expansion coefficient of SiO_2 is much larger than its thermo-optic coefficient, so the thermal expansion of the microresonator is the dominant factor in the spectral line shift. However, most

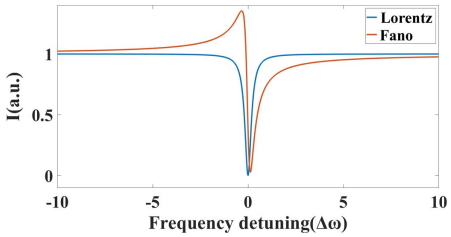

Fig. 1. Transmission spectra of the Lorentz resonance and the Fano resonance.

SiO_2 microresonators are nonhollow structures and cannot produce large deformations when temperature changes are small, which leads to the generally low sensitivity of temperature sensors based on ordinary SiO_2. Our proposed SHMR has a smaller wall thickness, which ensures the temperature sensor based on it has higher sensitivity.

Furthermore, for a given resonant wavelength λ, the variation of the normalized transmittance I of the resonant mode with temperature T can be expressed as[32]

$$\frac{\mathrm{d}I}{\mathrm{d}T} = \frac{\mathrm{d}I}{\mathrm{d}\lambda}\frac{\mathrm{d}\lambda}{\mathrm{d}T}, \tag{3}$$

where $\mathrm{d}\lambda/\mathrm{d}T$ is the conventional sensitivity and $\mathrm{d}I/\mathrm{d}\lambda$ is associated with the resonance line shape. As shown in Fig. 1, compared with the symmetric Lorentz line shape, the asymmetric Fano line shape has a larger slope ($\mathrm{d}I/\mathrm{d}\lambda$) near the central wavelength. Therefore, the Fano resonance excited by the SHMR can further improve the sensitivity of temperature sensing ($\mathrm{d}I/\mathrm{d}T$).

3. Experiment

We focus the CO_2 laser on a very small spot and melt-burn a high-speed rotating prefabricated SiO_2 hollow rod (with an outer diameter of 2 mm and an inner diameter of 1 mm) to prepare the SiO_2 microrod resonator with a hollow interior and a controllable wall thickness (within 0.5 mm). The details of the processing method are described in Ref. [33]. The maximum axial width of the microresonator is within 0.2 mm, and the surface curvature of the microresonator can be controlled by adjusting the CO_2 laser power. The maximum diameter of the SHMR shown in Fig. 2 is 1.547 mm. Compared with other forms of microresonators, the SHMR not only has a higher Q factor (3.16×10^7), but also has the following excellent properties:

1) The surface curvature of the SHMR is extremely large, and its axial width is small. Compared with microsphere microresonators, the SHMR has extremely concise resonance modes, which are conducive to the identification and analysis of the optical mode and can improve sensor performance.
2) The SHMR has a smaller wall thickness than a solid microresonator. When the force or temperature changes, the resulting deformation will be large and easy to detect,

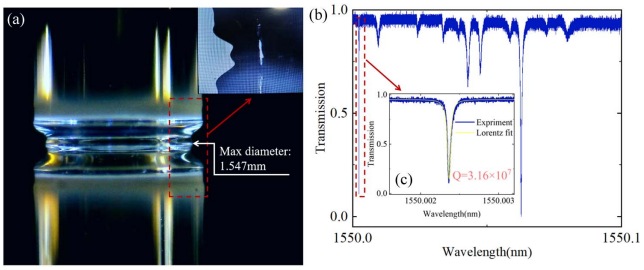

Fig. 2. (a) Image of SHMR; (b) transmission spectrum of SHMR coupled with tapered fiber; (c) Lorentz fitting of resonance peak.

which can effectively improve the measurement sensitivity.

3) Its hollow tube will enable the SHMR to directly come in contact with the experimental supplies without sacrificing its optical performance and thus can be used in numerous application scenarios.

The structure of the high-sensitivity temperature-sensing experimental system based on the high-Q-factor SHMR is shown in Fig. 3. The tunable laser, with a center wavelength of 1550 nm, is modulated by a triangular wave generated by an arbitrary waveform generator, then passes through a variable optical attenuator and a polarization controller. After the SHMR is coupled with a tapered fiber, the resonant output is detected by a photodetector, which is connected to an oscilloscope (OSC) to display the transmission spectrum.

In the experiment, we placed the heating resistor wire and the temperature-sensing probe of the temperature controller in the hollow tube of the SHMR, which made the temperature control system simple and reliable; the microresonator was heated more uniformly, the temperature changed more rapidly, and the temperature feedback was more accurate. Most importantly, the procedure did not affect the optical performance of the SHMR. By changing the power of the temperature controller, we can observe a shift of the transmission in the OSC and obtain the temperature-sensing response of the SHMR.

We use the SHMR in Fig. 2 to couple at the larger diameter of the tapered fiber to excite high-Q resonance. To ensure the stability of the coupled state during the experiment, we reduce the coupling spacing between the microresonator and the tapered fiber by a high-precision 3D translation stage to put them both

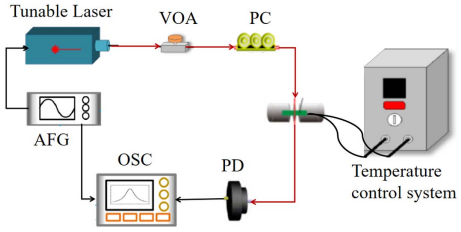

Fig. 3. Experimental temperature-sensing device. VOA, variable optical attenuator; PC, polarization controller; PD, photoelectric detector; OSC, oscilloscope; AFG, arbitrary waveform generator.

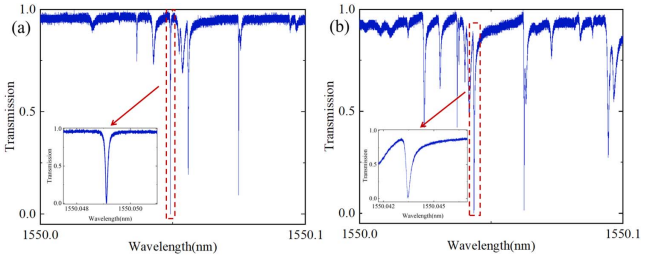

Fig. 4. (a) Lorentz resonance spectrum and target resonance peak in temperature sensing; (b) Fano resonance spectrum and target resonance peak in temperature sensing.

exactly in contact; the stable Lorentz resonance is excited as shown in Fig. 4(a). Subsequently, the coupling spacing continues to be reduced to keep the microresonator in contact with the tapered fiber, and the microresonator is slowly moved along the direction of decreasing diameter of the tapered fiber to excite the stable Fano resonance, as shown in Fig. 4(b). The transmission spectrum remains highly concise, with clear and easy-to-identify modes, thereby making it convenient for resonance peak identification and tracking.

4. Temperature Sensing Based on Lorentz Resonance

After exciting the stable Lorentz resonance, as shown in Fig. 4(a), we used the temperature control system to gradually heat the microresonator and observed the redshift of the resonance spectral line in the OSC. When we increased the microresonator temperature from 24.6 to 26.6°C, the resonance spectral line moved 49.80 pm toward the long wavelength direction, and Fig. 5(a) demonstrates the redshift of the target resonance peak at increments of 0.4°C, starting from 24.6°C. After

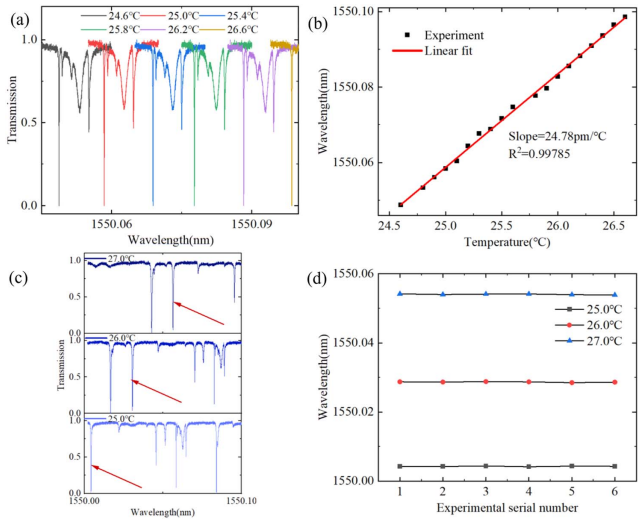

Fig. 5. (a) Temperature-sensing characteristics of SHMR under Lorentz resonance; (b) linear fit of resonance peak wavelength versus temperature; (c) Lorentz resonance spectrum in repeatable experiments; (d) wavelengths of target resonance peaks in six repeatable experiments.

Table 1. *Q* factors of Lorentz Resonance Peaks at Different Temperatures.

T (°C)	*Q* factor	*T* (°C)	*Q* factor
24.6	2.05×10^7	25.8	2.06×10^7
25.0	1.86×10^7	26.2	1.89×10^7
25.4	2.10×10^7	26.6	1.97×10^7

stopping the heating, the temperature of the microresonator decreases rapidly, and the resonance spectrum returns to the initial state. We performed a linear fitting of the relationship between the resonance peak wavelength and the temperature; the results are shown in Fig. 5(b), where the slope of the fitted straight line is 24.78 pm/°C, and $R^2 = 0.99785$. The experimental results demonstrate that an excellent linear relationship exists between the wavelength shift of the resonance peak and the degree of temperature variation. The temperature sensor based on Lorentz resonance excited in the SHMR demonstrates high sensitivity.

To verify the reliability and repeatability of the sensing system, we tested multiple temperature measurement cycles. We recorded the Lorentz resonance spectrum [Fig. 5(c)] at three temperature points (25, 26, and 27°C), then recorded the wavelengths of the target resonance peak in Fig. 5(d). The interval between each test was 20 min to allow the temperature of the microresonator to stabilize. The dot-line plot in Fig. 5(d) shows that the target resonance peak wavelengths at the same temperature point have satisfactory consistency. When we increase the microresonator temperature from 25 to 26°C, the average value of the target resonance peak wavelength shift is 24.39 pm, and the standard deviation is 0.133 pm. When we increase the microresonator temperature from 25 to 27°C, the average value of the target resonance peak wavelength shift is 49.75 pm, with a standard deviation of 0.159 pm, which indicates that the sensing system has satisfactory reliability and repeatability.

In order to intuitively evaluate the effect of temperature change on the *Q* factor of the microresonator, we estimated the *Q* factor of the target resonance peak in Fig. 5(a). As shown in Table 1, the *Q* factor fluctuates in a very small range, and the effect of temperature change on the *Q* factor of the microresonator can be ignored within the allowable error range.

5. Temperature Sensing Based on Fano Resonance

Subsequently, we excited the stable Fano resonance again, as shown in Fig. 4(b), and gradually increased the temperature of the microresonator using the temperature control system. We observed the redshift phenomenon of the resonance spectral line in the OSC. When we increased the microresonator temperature from 24.5 to 26.2°C, the resonance spectral line shifted 52.99 pm toward the long wavelength direction. Figure 6(a) demonstrates the redshift of the target resonance peak at

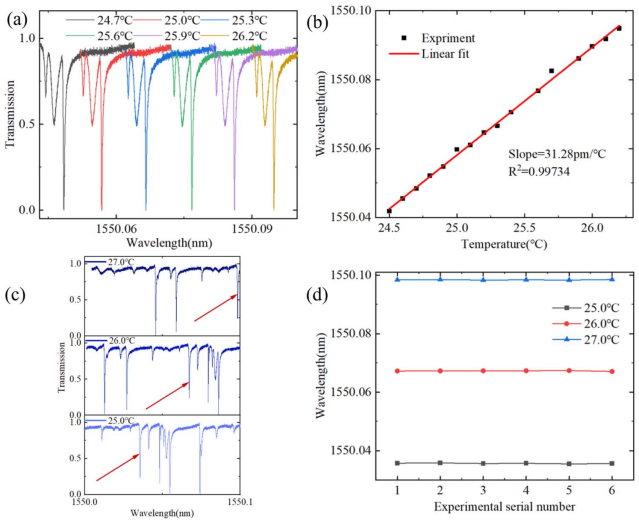

Fig. 6. (a) Temperature-sensing characteristics of SHMR under Fano resonance; (b) linear fit of resonance peak wavelength versus temperature; (c) Fano resonance spectrum in repeatable experiments; (d) wavelengths of target resonance peaks in six repeatable experiments.

increments of 0.3°C, starting from 24.7°C. After stopping the heating, the temperature of the microresonator decreases rapidly, and the resonance spectral line returns to the initial state. Similarly, we performed a linear fitting of the relationship between the resonance peak wavelength and the temperature; the fitting results are shown in Fig. 6(b), where the slope of the fitted straight line is 31.28 pm/°C, and $R^2 = 0.99734$. The experiment proves that an excellent linear relationship exists between the resonance peak wavelength shift and the temperature variation, and the temperature sensor based on Fano resonance excited in the SHMR has high sensitivity.

We also conducted six experiments at three temperature points to verify the reliability and repeatability of the sensing system, with a 20 min interval between each experiment. The Fano resonance spectrum and the wavelengths of the target resonance peak in the experiments are shown in Figs. 6(c) and 6(d). The wavelengths of the target resonance peak at the same temperature points also demonstrate satisfactory consistency. When we increase the microresonator temperature from 25 to 26°C, the average value of the target resonance peak wavelength shift is 31.62 pm, with a standard deviation of 0.168 pm. When we increase the microresonator temperature from 25 to 27°C, the average value of the target resonance peak wavelength shift is 62.76 pm, with a standard deviation of 0.114 pm, which indicates the satisfactory reliability and reproducibility of the sensing system.

We also estimated the *Q* factor of the target resonance peak in Fig. 6(a), as shown in Table 2. Under the premise of ignoring the reading error, it can be considered that the *Q* factor remains basically unchanged. This is because the microresonator and the tapered fiber are in an overcoupled state, making the resonance mode stable. This also indirectly reflects that the sensing system based on Fano resonance has better stability.

Table 2. *Q* Factors of Fano Resonance Peaks at Different Temperatures.

T (°C)	*Q* factor	*T* (°C)	*Q* factor
24.7	4.08×10^6	25.6	4.23×10^6
25.0	4.19×10^6	25.9	4.19×10^6
25.3	4.19×10^6	26.2	4.23×10^6

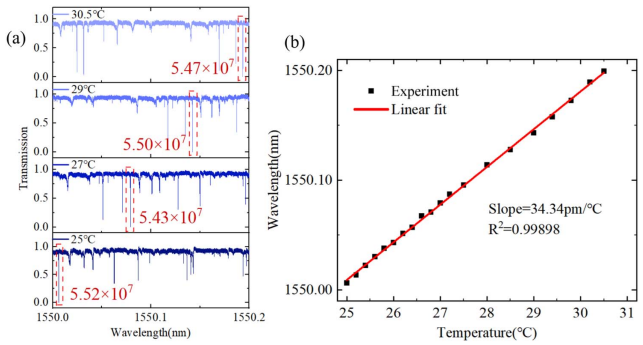

Fig. 7. Temperature-sensing characteristics after further reduction of resonator wall thickness.

6. Further Reduction of Resonator Wall Thickness

To further verify the effectiveness of reducing the wall thickness of the SHMR in improving the temperature sensing sensitivity, we used a SiO_2 hollow rod with an outer diameter of 1 mm and an inner diameter of 0.5 mm to prepare a high-*Q* SHMR, and again performed temperature-sensing experiments under the Lorentz resonance. The results are shown in Fig. 7; the *Q* factor of the target resonance peak still fluctuates within a small range. When the microresonator temperature increases from 25 to 30.5°C, the resonance spectrum shifts by 193.27 pm toward the long wavelength direction. The slope of the fitted line between the resonance peak wavelength and temperature is 34.34 pm/°C, and $R^2 = 0.99898$. The experiment proves that reducing the wall thickness of the SHMR can effectively improve the temperature-sensing sensitivity.

7. Discussion

Throughout the entire experimental process, the profile of the resonance spectral line did not change considerably with the temperature change, and we observed an excellent linear relationship between the experimentally measured resonant peak wavelength shift and the temperature change. Moreover, the system demonstrates satisfactory repeatability and reliability. The experimental results show that, without changing the thermo-optical coefficient of the microresonator, the sensitivity of the temperature sensor based on the SHMR can be improved several times higher than that of sensors based on ordinary SiO_2 microresonators. Sensitivity reaches 24.78 pm/°C under Lorentz resonance, whereas the reported sensitivity of temperature-sensing systems based on ordinary SiO_2 microbottle cavities[18,19], microsphere cavities[21], etc. is less than 11 pm/°C. A comparison is shown in Table 3. When we utilize Fano resonance excited in the SHMR for temperature sensing, the sensitivity of the temperature sensor in this study is improved by nearly 30% to 31.28 pm/°C, which can be attributed to the sharp slope (large $dI/d\lambda$) of Fano resonance. In addition, the wall thickness of the SHMR can be further reduced using thinner hollow SiO_2 rods, which improves the sensitivity of the temperature sensor in this study to 34.34 pm/°C under Lorentz resonance.

Table 3. Sensitivity Comparison of SiO_2 Microresonator Temperature-Sensing Systems.

Structure	*Q* factor	Sensitivity (pm/°C)	Year/Ref.
SiO_2 microbottle	10^5	1.3	2019[18]
SiO_2 microsphere	4.1×10^4	7.38	2020[21]
SiO_2 microbottle	7.4×10^6	10.5	2018[19]
SiO_2 hollow microrod	5.5×10^7	34.3	This work

8. Conclusion

In this study, we fabricated a thin-walled SHMR with a high *Q* factor and extremely concise resonance modes. The temperature sensor based on the SHMR has higher sensitivity owing to the small wall thickness of the SHMR, and also demonstrates satisfactory stability, reliability, and repeatability. Compared with the sensitivity of an ordinary SiO_2 microresonator temperature sensor, the sensitivity of the SHMR is improved several times, reaching 24.78 pm/°C under Lorentz resonance and further improved to 31.28 pm/°C under Fano resonance. Further reducing the wall thickness of the SHMR, the sensitivity under Lorentz resonance is improved to 34.34 pm/°C. Our experiments show that reducing the wall thickness of the microresonator and using Fano resonance excited in the microresonator can enhance the sensitivity of SiO_2 microresonator temperature sensors. In addition, the microresonator sensor in this study is simple to fabricate, low cost, reliable, and highly sensitive, and has satisfactory application value in the field of temperature sensing.

Acknowledgements

This work was supported by the Fundamental Research Funds for the Central Universities (Nos. JZ2023HGQA0106 and JZ2023HGTA0199) and the Anhui Provincial Natural Science Foundation (No. 2308085QF208).

References

1. S. Yang, Y. Wang, and H. Sun, "Advances and prospects for whispering gallery mode microcavities," Adv. Opt. Mater. **3**, 1136 (2015).

2. J. U. Fürst, K. Buse, I. Breunig, *et al.*, "Second-harmonic generation of light at 245 nm in a lithium tetraborate whispering gallery resonator," Opt. Lett. **40**, 1932 (2015).
3. N. G. Pavlov, S. Koptyaev, G. V. Lihachev, *et al.*, "Narrow-linewidth lasing and soliton Kerr microcombs with ordinary laser diodes," Nat. Photonics **12**, 694 (2018).
4. H. K. Hunt and A. M. Armani, "Bioconjugation strategies for label-free optical microcavity sensors," IEEE J. Sel. Top. Quantum Electron. **20**, 121 (2013).
5. J. L. Nadeau, V. S. Iltchenko, D. Kossakovski, *et al.*, "High-Q whispering-gallery mode sensor in liquids," in *Conference on Laser Resonators and Beam Control V Jan 22–23* (2002).
6. N. Toropov, G. Cabello, M. P. Serrano, *et al.*, "Review of biosensing with whispering-gallery mode lasers," Light Sci. Appl. **10**, 42 (2021).
7. J. Bian, T. Lang, W. Kong, *et al.*, "A polarization maintaining fiber sensor for simultaneous measurement of temperature and strain," Optik **127**, 10090 (2016).
8. B.-B. Li, D. Bulla, V. Prakash, *et al.*, "Invited article: scalable high-sensitivity optomechanical magnetometers on a chip," APL Photon. **3**, 120806 (2018).
9. Y. Liu, H. Zhang, M. Fan, *et al.*, "Bidirectional tuning of whispering gallery modes in a silica microbubble infiltrated with magnetic fluids," Appl. Opt. **59**, 1 (2020).
10. W. Xu, C. Xu, F. Qin, *et al.*, "Whispering-gallery mode lasing from polymer microsphere for humidity sensing," Chin. Opt. Lett. **16**, 081401 (2018).
11. A. Savchenkov, A. Matsko, D. Strekalov, *et al.*, "Mode filtering in optical whispering gallery resonators," Electron. Lett. **41**, 495 (2005).
12. G. S. Murugan, J. S. Wilkinson, and M. N. Zervas, "Selective excitation of whispering gallery modes in a novel bottle microresonator," Opt. Express **17**, 11916 (2009).
13. W. Meng-Yu, M. Ling-Jun, Y. Yu, *et al.*, "Selection of whispering-gallery modes and Fano resonance of prolate microbottle resonators," Acta Phys. Sin. **69**, 234203 (2020).
14. M. Pöllinger, D. O'Shea, F. Warken, *et al.*, "Ultrahigh-Q tunable whispering-gallery-mode microresonator," Phys. Rev. Lett. **103**, 053901 (2009).
15. M. N. M. Nasir, M. Ding, G. S. Murugan, *et al.*, "Microtaper fiber excitation effects in bottle microresonators," in *Laser Resonators, Microresonators, and Beam Control XV* (2013), p. 229.
16. Y. Yin, Y. Niu, M. Ren, *et al.*, "Strain sensing based on a microbottle resonator with cleaned-up spectrum," Opt. Lett. **43**, 4715 (2018).
17. J. Liao, X. Wu, L. Liu, *et al.*, "Fano resonance and improved sensing performance in a spectral-simplified optofluidic micro-bubble resonator by introducing selective modal losses," Opt. Express **24**, 8574 (2016).
18. M. Batumalay, M. A. M. Johari, M. I. M. A. Khudus, *et al.*, "Microbottle resonator for temperature sensing," J. Phys. **1371**, 012006 (2019).
19. J. Herter, V. Wunderlich, C. Janeczka, *et al.*, "Experimental demonstration of temperature sensing with packaged glass bottle microresonators," Sensors **18**, 4321 (2018).
20. J. M. Ward, Y. Yang, and S. Nic Chormaic, "Glass-on-glass fabrication of bottle-shaped tunable microlasers and their applications," Sci. Rep. **6**, 25152 (2016).
21. Y.-N. Zhang, N. Zhu, T. Zhou, *et al.*, "Research on fabrication and sensing properties of fiber-coupled whispering gallery mode microsphere resonator," IEEE Sens. J. **20**, 833 (2019).
22. J.-L. Kou, S.-J. Qiu, F. Xu, *et al.*, "Demonstration of a compact temperature sensor based on first-order Bragg grating in a tapered fiber probe," Opt. Express **19**, 18452 (2011).
23. C.-H. Dong, L. He, Y.-F. Xiao, *et al.*, "Fabrication of high-Q polydimethylsiloxane optical microspheres for thermal sensing," Appl. Phys. Lett. **94**, 231119 (2009).
24. L. He, Y.-F. Xiao, C. Dong, *et al.*, "Compensation of thermal refraction effect in high-Q toroidal microresonator by polydimethylsiloxane coating," Appl. Phys. Lett. **93**, 201102 (2008).
25. B.-B. Li, Q.-Y. Wang, Y.-F. Xiao, *et al.*, "On chip, high-sensitivity thermal sensor based on high-Q polydimethylsiloxane-coated microresonator," Appl. Phys. Lett. **96**, 251109 (2010).
26. Y.-L. Shang, M.-Y. Ye, and X.-M. Lin, "Experimental observation of Fano-like resonance in a whispering-gallery-mode microresonator in aqueous environment," Photon. Res. **5**, 119 (2017).
27. X. Jin, H. Liu, X. Xu, *et al.*, "Dynamic Fano resonance and enhanced harmful gas measurement sensitivity in a universal multimode waveguide-microcavity model," Opt. Eng. **61**, 061403 (2022).
28. J. Hu, X. Liu, J. Zhao, *et al.*, "Investigation of Fano resonance in compound resonant waveguide gratings for optical sensing," Chin. Opt. Lett. **15**, 030502 (2017).
29. F. Lei, B. Peng, S. K. Oezdemir, *et al.*, "Dynamic Fano-like resonances in erbium-doped whispering-gallery-mode microresonators," Appl. Phys. Lett. **105**, 1866 (2014).
30. T. Carmon, L. Yang, and K. J. Vahala, "Dynamical thermal behavior and thermal self-stability of microcavities," Opt. Express **12**, 4742 (2004).
31. L. Xu, X. Jiang, G. Zhao, *et al.*, "High-Q silk fibroin whispering gallery microresonator," Opt. Express **24**, 20825 (2016).
32. J. Li, R. Yu, C. Ding, *et al.*, "PT-symmetry-induced evolution of sharp asymmetric line shapes and high-sensitivity refractive index sensors in a three-cavity array," Phys. Rev. A **93**, 023814 (2016).
33. S. B. Papp, P. Del'Haye, and S. A. Diddams, "Mechanical control of a microrod-resonator optical frequency comb," Phys. Rev. X **3**, 031003 (2013).